JOURNAL OF MATERIALS SCIENCE 20 (1985) 3545–3556

Development of microstructure during the fabrication of Si_3N_4 by nitridation and pressureless sintering of $Si:Si_3N_4$ compacts

L. K. L. FALK, R. POMPE*, G. L. DUNLOP
Department of Physics, Chalmers University of Technology and
**Swedish Institute for Silicate Research, S–412 96 Göteborg, Sweden*

The technique for the fabrication of Si_3N_4 which was investigated involves the nitridation of $Si:Si_3N_4$ powder compacts containing additions of sintering aids (e.g. Y_2O_3 and Al_2O_3) followed by pressureless sintering. The development of microstructure during fabrication by this method has been followed by X-ray diffraction and analytical electron microscopy. As well as being important for the sintering process, it was found that the sintering aids promote nitridation through reaction with the surface silica on the powder particles. During nitridation extremely fine grained Si_3N_4 forms at silicon powder particle surfaces and at tunnel walls extending into the interior of these powder particles. Secondary crystalline phases which form during nitridation are eliminated from the microstructure during sintering. The α- to β-Si_3N_4 phase transformation is completed early in the sintering process, but despite this the fully sintered product contains fine β-Si_3N_4 grains. The β grains are surrounded by a thin intergranular amorphous film.

1. Introduction

Recently a new method for the fabrication of dense Si_3N_4 material has been developed which involves the nitridation and subsequent pressureless sintering of submicron silicon and Si_3N_4 powder compacts containing additions of sintering aids [1, 2]. The powder compacts are nitrided in nitrogen gas at atmospheric pressure and at temperatures in the range 1260 to 1400° C. This is followed by pressureless sintering of the nitrided compacts at 1850° C. A detailed description of the process is given in [1].

In order for this process to function satisfactorily it is important that, prior to nitridation, the starting powders are submicron in grain size and that the different starting species are intimately mixed. This is achieved by milling all of the starting powders (silicon, Si_3N_4 and sintering aids) together. During milling the Si_3N_4 powder particles act as a dispersant which facilitates the milling of the silicon powder to a submicron size. The powder mixture which is so obtained can be formed into powder compacts by cold isostatic pressing or by other forming methods.

The nitridation/pressureless sintering technique appears to have several advantages compared to other existing processes for the fabrication of dense and complex shaped Si_3N_4 bodies. The mixture of the submicron silicon and Si_3N_4 powders in the compacts enables the use of considerably shorter nitridation times than is required for sintered reaction-bonded Si_3N_4 [3]. The green bodies after nitriding have a relatively high density (approximately 70% of the theoretical), which reduces the linear shrinkage during sintering to approximately 10%. The weight loss during sintering is also minimized due to the reduced pore volume in nitrided

0022–2461/85 $03.00 + .12

material. The nitrided powder compacts prior to sintering have a reasonable mechanical strength but have a low abrasion resistance, which allows them to be machined to close tolerances. The possibility of reduced production costs due to the usage of cheaper raw materials (i.e. silicon powder) is also an advantage.

The present paper is concerned with the detailed development of microstructure during fabrication of the Si_3N_4 material by the nitriding/pressureless sintering technique. Attention has been given to the influence of different processing parameters on the resultant microstructure.

2. Experimental details

2.1. Material preparation

The submicron powder compacts prepared for the present investigation had a $Si:Si_3N_4$ mass ratio of 6:4 and contained Y_2O_3 and Al_2O_3 as sintering aids. The amount of sintering aids added was such that the compacts contained 6 wt % Y_2O_3 and 2 wt % Al_2O_3 after full nitridation. The submicron Si_3N_4 powder used was H.C. Starck quality LC 10. The starting silicon powder was coarser, with a particle size of up to 300 μm and had an impurity content of approximately (wt %) 0.4 Fe, 0.4 O, 0.2 Al and 0.1 Ca. Mixtures of the Si_3N_4 and silicon powders and the sintering aids were prepared by wet milling in ethanol for 15 to 20 h in a planetary agate ball mill with agate balls. This milling operation resulted in a substantial reduction of the particle size of the silicon powder.

Powder compacts were formed by cold isostatic pressing at a pressure of 280 MPa resulting in a green body density which was approximately 60% of the theoretical. These powder compacts were then nitrided at different temperatures in the range 1260 to 1400° C.

Nitridation was carried out in nitrogen gas at atmospheric pressure. The reaction path during the nitriding process was investigated using a Mettler thermobalance (TA1) and a Harrope sintering dilatometer (TD–760). After nitridation the powder compacts had a density of approximately 70% of the theoretical. The pressureless sintering of powder compacts, which had been fully nitrided at 1350° C, was carried out at 1850° C with the compacts surrounded by a Si_3N_4 powder bed and under a nitrogen gas atmosphere. A more detailed description of the preparation of the powder compacts and the experimental procedure during nitriding and sintering is given in [1].

2.2. Microstructural analysis

The microstructures of nitrided and sintered material were characterized by X-ray diffractometry and analytical electron microscopy using scanning and transmission microscopy (SEM, TEM, STEM) with energy-dispersive analysis of X-rays (EDX).

Thin foils for TEM and STEM were prepared from ~0.5 mm thin slices cut by a high-speed diamond saw. These slices were ground on SiC grinding paper to a thickness of 60 to 80 μm. The final thinning was carried out by ion-beam milling with a 5 kV argon-ion beam incident on both surfaces of the foil at an angle of 30°. To avoid charging in the electron microscope, a thin carbon film was vacuum evaporated on to the foil surface. The thin foils were investigated in a JEOL 200CX TEM/STEM instrument with an attached Link 860 EDX system.

Room-temperature fracture surfaces of nitrided material were prepared for scanning electron microscopy (SEM). These samples were also coated with carbon in order to avoid charging in the microscope.

Peak height ratios from X-ray diffractograms were used to determine relative changes in phase content in the compacts during the nitridation and sintering processes.

3. Results

3.1. Nitridation

3.1.1. The structure of fully nitrided compacts

X-ray diffraction of nitrided material showed that both α- and β-Si_3N_4, Y–N–apatite and an yttrium silicate (Y_2SiO_5) are formed during the nitridation process. The relative amounts of these different phases present in nitrided bodies were dependent upon the temperature of nitridation. Peak height ratios from X-ray diffractograms obtained from powder compacts nitrided at different temperatures revealed the relatively strong changes in the proportion of α- and β-Si_3N_4 shown in Fig. 1. At temperatures up to 1350° C the $\alpha/(\alpha + \beta)$ peak height ratio was approximately constant, but at higher nitridation temperatures the β-phase content increased.

Scanning electron micrographs of room-

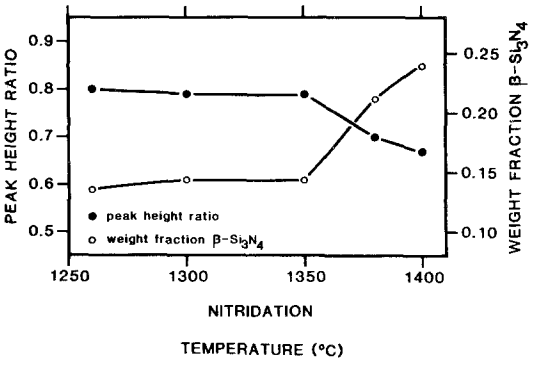

Figure 1 $\alpha/(\alpha + \beta)$ Si_3N_4 peak height ratios measured from X-ray diffractograms of powder compacts which were fully nitrided at the temperatures indicated. The curve indicating the weight fraction $\beta/(\alpha + \beta)$ was obtained using data provided by [4].

temperature fracture surfaces of compacts nitrided at different temperatures are shown in Fig. 2. All of the fracture surfaces contained continuous smooth areas which increased in size with increasing nitridation temperature. Often these smooth areas surrounded pores in the microstructure. The presence of this morphology suggested that there were amorphous regions in the microstructure of nitrided powder compacts. The amount of this amorphous phase apparently increased with increasing nitriding temperature.

Despite the porous structure of the nitrided bodies, it was possible to prepare thin foils for transmission electron microscopy (TEM). The microstructure of the nitrided powder compacts

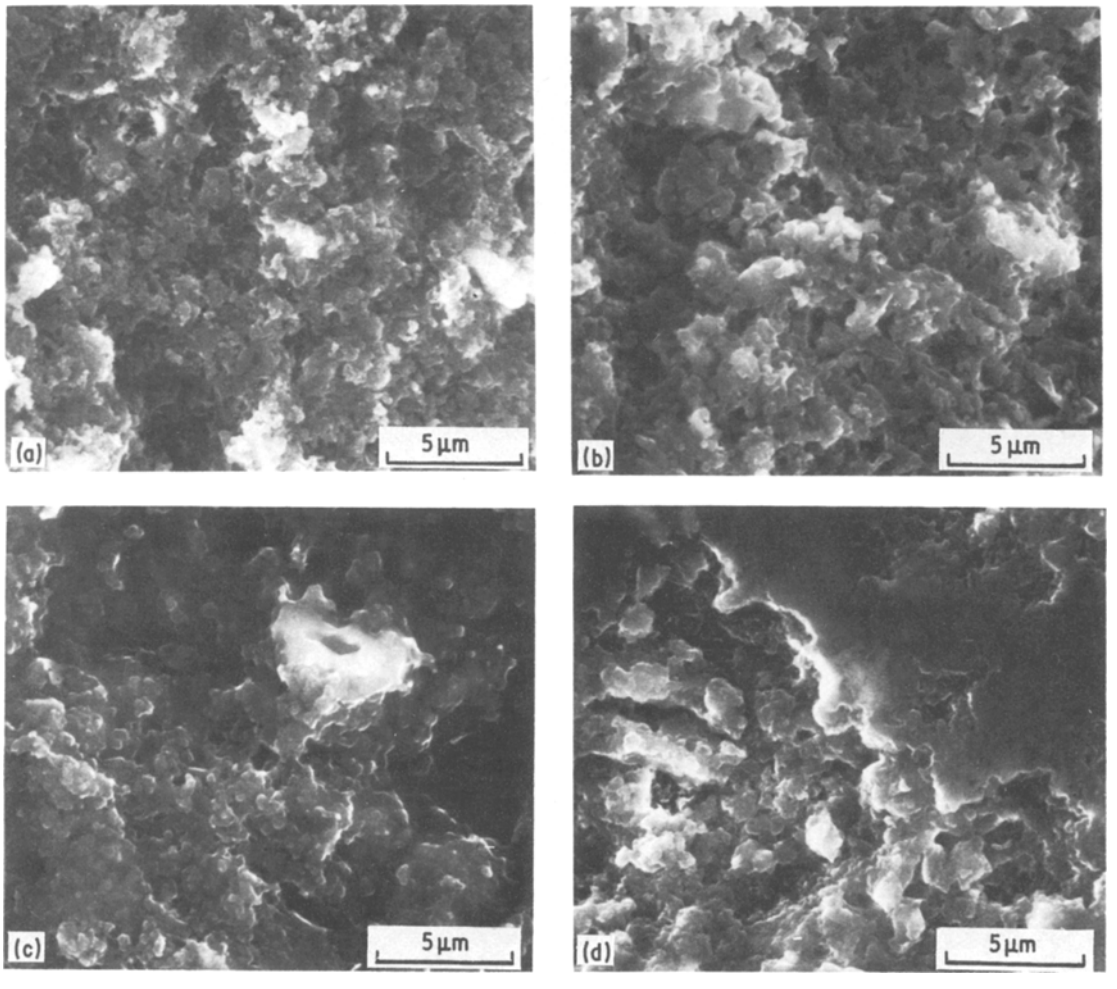

Figure 2 Scanning electron micrographs of room-temperature fracture surfaces of compacts which were fully nitrided at (a) 1260° C; (b) 1350° C; (c) 1380° C; (d) 1400° C.

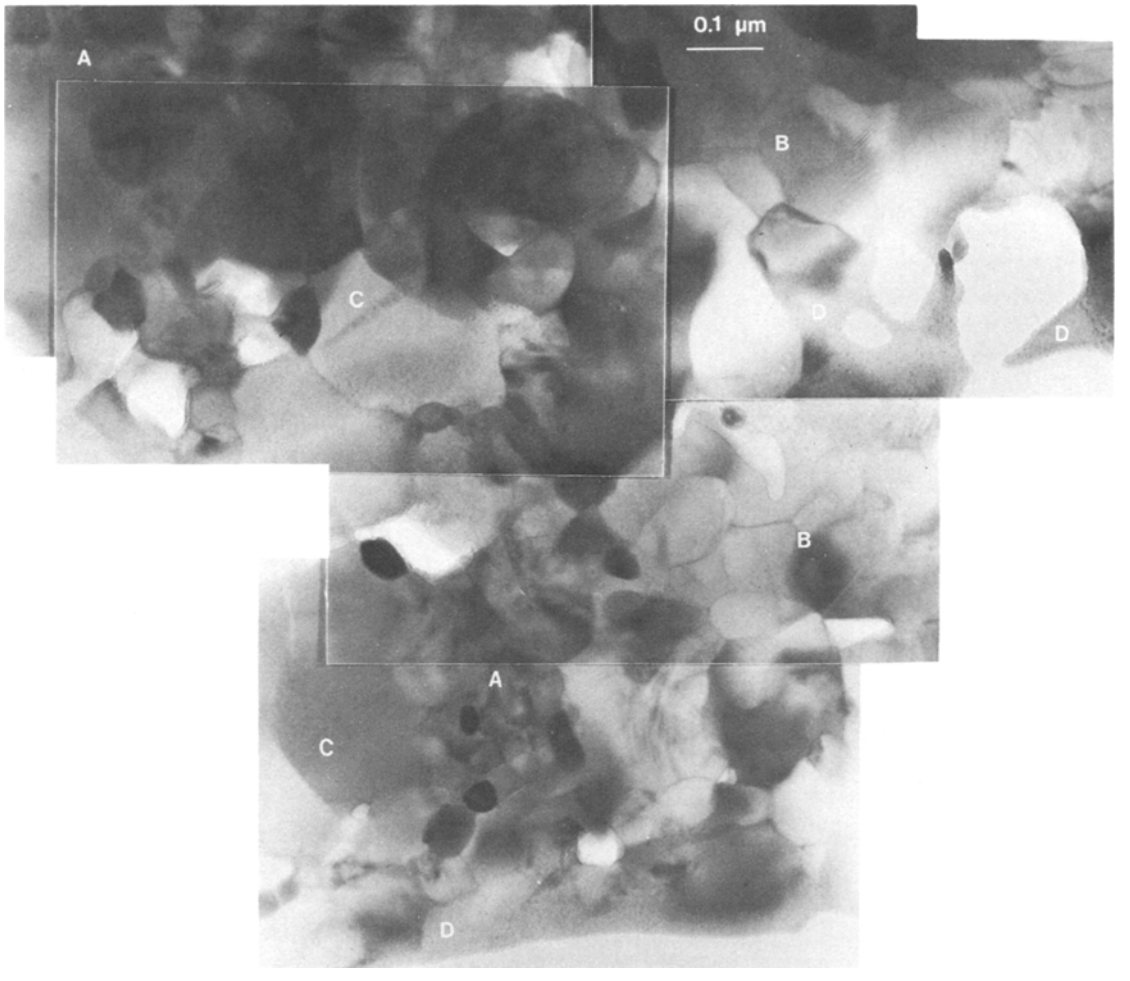

Figure 3 The microstructure of a fully nitrided powder compact. Note the wide distribution of grain sizes. Regions with fine (A) and intermediate (B) sized Si_3N_4 grains are probably Si_3N_4 which was formed during nitridation. The largest grains (C) are probably inherited from the original Si_3N_4 starting powder. An amorphous region (D) can be seen encompassing a hole in the thin foil.

contained, as shown in Fig. 3, some fine-grained areas where the Si_3N_4 grain size was 30 to 50 nm. As well as these fine-grained regions there also existed intermediate (50 to 200 nm) sized Si_3N_4 grains, which were surrounded by thin (2 to 5 nm) intergranular amorphous films (Fig. 4a) and often bounded by larger amorphous regions. It seems likely that both of these types of Si_3N_4 grains had formed during nitridation. In other parts of the microstructure fairly large grains were present (see also Fig. 3), which most likely were inherited from the Si_3N_4 starting powder. Secondary crystalline phases were observed at sites lying between large Si_3N_4 grains and also between the smaller grains (Fig. 4b). These crystalline phases strongly absorbed the electron beam, suggesting that they correspond to the Y_2SiO_5 and Y–N–apatite detected by X-ray diffraction.

The microstructure also contained large amorphous areas which generally surrounded small holes in the thin foils (Fig. 3). The amorphous nature of these areas could be readily determined by their lack of diffraction contast and susceptibility to radiation damage under the electron beam. Microanalysis by STEM/EDX detected only silicon in this amorphous phase. It is thought that the small holes in the amorphous regions correspond to pores in the nitrided body similar to those observed by SEM (Fig. 2).

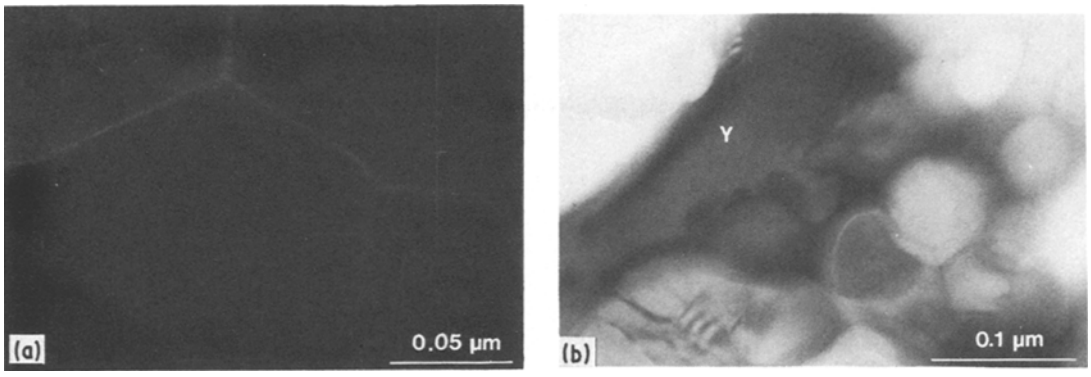

Figure 4 Intergranular phases in fully nitrided material: (a) thin intergranular amorphous film between the intermediate sized Si_3N_4 grains, shown in a dark-field micrograph using diffuse scattered electrons to form the image [5]; (b) a crystalline yttrium-rich phase (Y) bounding a fine-grained region.

3.1.2. The sequence of nitridation at 1350° C

In order to investigate the nitriding process in more detail, powder compacts were nitrided at 1350° C to different degrees of conversion of silicon to Si_3N_4. The time–temperature schedule used for nitriding is shown in Fig. 5, together with the thermogravimetric and dilatometric curves for the process. The different degrees of conversion of silicon to Si_3N_4 in the samples which were microstructurally characterized are also indicated in Fig. 5.

The relative changes in phase content in the powder compacts during the nitridation process at 1350° C can be seen in Fig. 6, which shows peak height ratios from X-ray diffractograms as a function of the degree of conversion of silicon to Si_3N_4. The volume fractions of both α-Si_3N_4 and β-Si_3N_4 in the compacts increased during the nitridation process, and as the conversion of silicon to Si_3N_4 proceeded the proportion of β-Si_3N_4 relative to α-Si_3N_4 increased. It was also found that powder compacts, which were held at the nitridation temperature for times longer than that required for full conversion of silicon to Si_3N_4, did not exhibit any detectable changes in the relative amounts of α and β-Si_3N_4.

The yttrium silicate Y_2SiO_5 was formed very early in the process, and after only a small amount of conversion of silicon to Si_3N_4 the formation of Y–N–apatite began. Towards the end of nitriding the amount of apatite increased and there was a slight decrease in the yttrium silicate content. X-ray diffraction also showed that the amount of Y_2O_3 in the compacts decreased rapidly during the early stages of nitridation such that after 12% conversion of silicon to Si_3N_4 no peaks from Y_2O_3 could be readily detected in the X-ray diffractograms.

SEM of room-temperature fracture surfaces

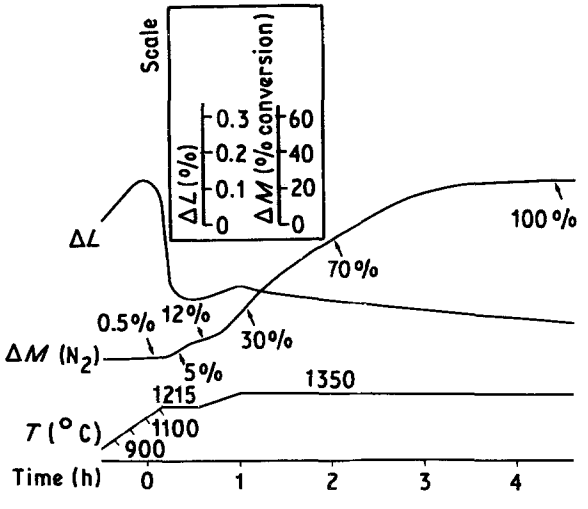

Figure 5 The time–temperature programme used for nitridation at 1350° C. The thermogravimetric and dilatometric curves for the process are also shown. The different degrees of conversion of silicon to Si_3N_4 in the partially nitrided compacts which were microstructurally investigated are indicated on the thermogravimetric curve.

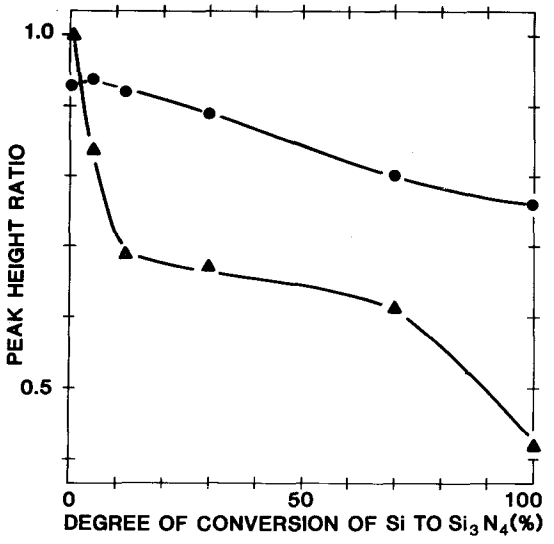

Figure 6 Peak height ratios from X-ray diffractograms as a function of the degree of conversion of silicon to Si_3N_4 when nitriding at 1350° C according to the time–temperature schedule shown in Fig. 5. ● α-Si_3N_4/(α-Si_3N_4 + β-Si_3N_4). ▲ yttrium silicate/(yttrium silicate + apatite).

from partially nitrided powder compacts suggested that phases which formed early in the nitridation process nucleated and grew on the original powder particles. This can be seen in Fig. 7, which shows a sequence of SEM micrographs of fracture surfaces of compacts which had been nitrided to various degrees of conversion of silicon to Si_3N_4. These new grains tended to agglomerate after longer nitridation times, and the large smooth areas mentioned previously (Fig. 2) also became readily apparent on fracture surfaces of compacts nitrided to a high degree of converstion (e.g. 70%) of silicon to Si_3N_4. These smooth areas, which surrounded pores in the microstructure, became larger as the nitriding process was brought to completion.

TEM of thin foils from a powder compact which had been nitrided to 70% conversion of silicon to Si_3N_4, showed that a fine-grained structure was present on the surface of the silicon grains (Fig. 8). The silicon grains also contained tunnels extending from the surface into the grain interiors, and the walls of these tunnels were covered with a fine-grained structure similar to that which was on the grain surfaces. Microanalysis of the small surface grains by STEM/EDX showed that they did not contain any detectable amounts of elements other than silicon. Interplanar spacings of these same small grains obtained by electron diffraction were consistent with them being α-Si_3N_4 and, possibly, β-Si_3N_4. Thus in this case, Si_3N_4 forms on the surface of the silicon grains during nitriding, and tunnels which penetrate the grain interiors also form. The walls of the tunnels then also serve as nucleation sites for new Si_3N_4 grains. The nitride grains form a surface layer which is even polycrystalline in a direction normal to the surface. This implies that new grains nucleated and grew on the original monocrystalline layer (~ 50 nm thick, see Fig. 8). In many cases an amorphous silicon-rich phase could be observed covering the fine-grained surface structure.

3.2. Microstructural changes during sintering

The development of microstructure during pressureless sintering at 1850° C was investigated in partially sintered powder compacts which had previously been fully nitrided at 1350° C according to the temperature schedule shown in Fig. 5. Sintering times together with densities, shrinkage and mass losses for the specimens which were investigated are given in Table I.

X-ray diffraction showed that virtually all of the α-Si_3N_4 present in the nitrided compacts transformed to β-Si_3N_4 during heating to 1840° C. No peaks corresponding to the α-phase could be detected in X-ray diffractograms from material held at the sintering temperature of 1850° C for five minutes or longer. Thus the α to β transformation takes place very early in the liquid phase sintering process for nitrided powder compacts prepared according to this method. During sintering, the volume fractions

TABLE I Sintering times for powder compacts fully nitrided at 1350° C and subsequently partially pressureless sintered at 1850° C

Sintering time (min)	Density (% of theoretical value)*	Shrinkage $-\Delta\bar{l}$ (%)	Mass loss $-\Delta m$ (%)
0 (1840° C)	77	2.9	0
5	82	4.1	0
25	92	7.9	0.7
125	98	10.2	0.9
250	99.5	10.5	1.1

*Density of nitrided bodies prior to sintering 71% of theoretical.

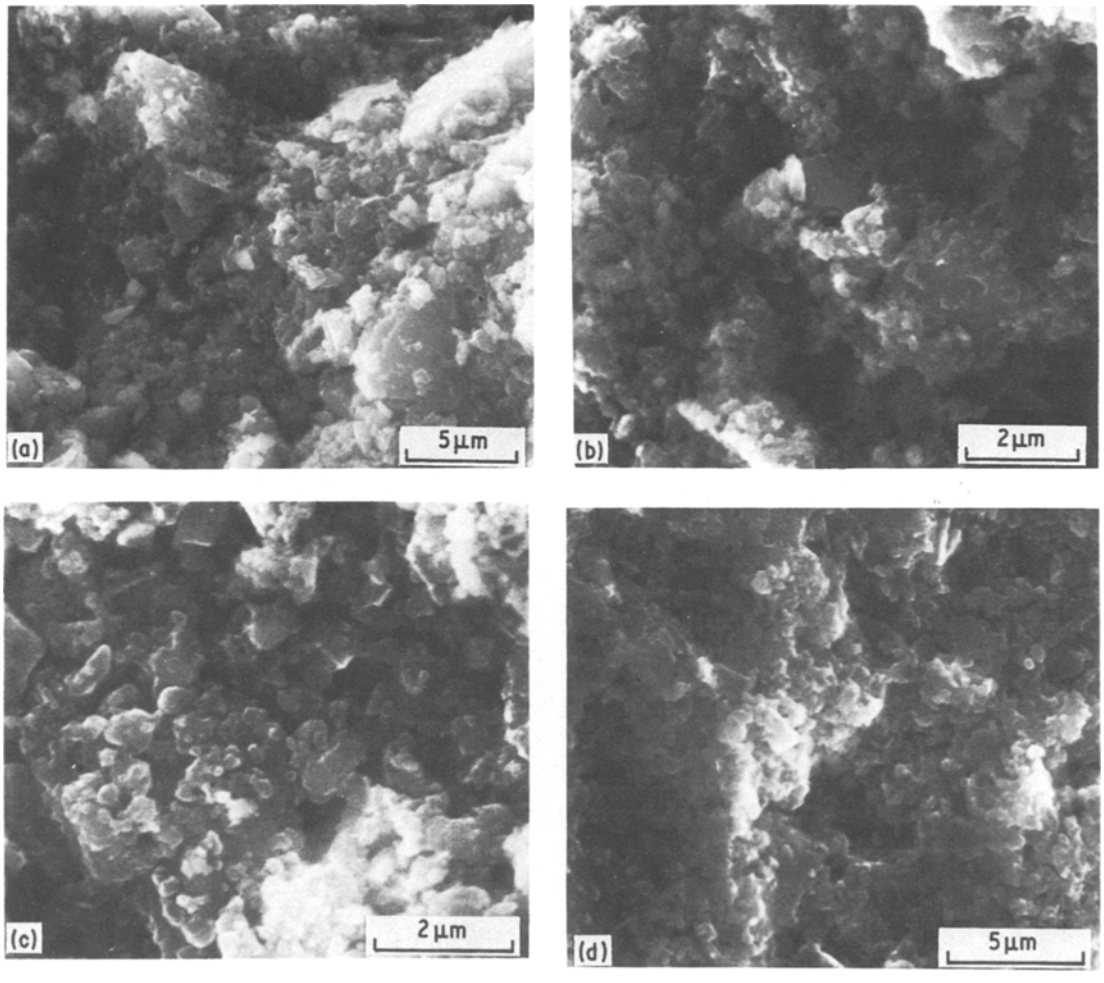

Figure 7 SEM of room-temperature fracture surfaces from powder compacts partially nitrided at 1350° C: (a) 0.5%; (b) 12%; (c) 30%; (d) 70% conversion of silicon to Si_3N_4.

of both the Y–N–apatite and the yttrium silicate phases decreased and X-ray diffraction of fully sintered material showed that these secondary crystalline phases were absent from the final product.

TEM of partially sintered material showed that the main microstructural constituent was β-Si_3N_4 whose grain size varied strongly (Fig. 9). The β-Si_3N_4 grains were surrounded by an amorphous phase which was present both as a thin intergranular film (~ 2 nm thick) and as larger pockets. Microanalysis of large glass pockets at intermediate stages of sintering (25 min and 2 h) by STEM/EDX showed that the glass was rich in silicon, yttrium and aluminium and indicated large variations in composition between different areas. The secondary crystalline phases in partially sintered material were usually situated at triple junctions, where they were surrounded by the amorphous phase.

Fine-grained features (diameter $\sim 0.5\,\mu$m) such as that shown in Fig. 10 were found in some glass pockets. A limited number of these features could also be observed in fully sintered material. Microanalysis by STEM/EDX (Fig. 10b) showed that they had a high impurity content. The especially high iron content originates from the silicon starting powder, which contained approximately 0.4 wt % Fe. The glass phase which surrounded these features did not contain any detectable amounts of these impurities.

Small β-Si_3N_4 grains with a near-spherical shape, which were present in larger glass pockets (Fig. 11) were relatively common in partially sintered material and were also present to a lesser extent in the microstructure of fully

Figure 8 A silicon powder particle at an early stage of nitridation at 1350° C. Note the tunnels extending from the particle surface into its interior. The fine-grained surface layer and tunnel walls are probably newly formed Si_3N_4 grains. A thin amorphous layer (A) is coating the fine-grained structure.

sintered bodies. It would seem that these were β-Si_3N_4 grains in the process of dissolution. The larger β-Si_3N_4 grains bordering these pockets had a faceted shape which is characteristic for grains which have grown in an isotropic liquid phase. These observations indicate that Ostwald ripening takes place during liquid-phase sintering.

3.3. Microstructure of fully sintered material

X-ray diffraction combined with TEM showed that the microstructure of fully sintered material consisted of β-Si_3N_4 grains which were in many cases hexagonal in cross-section and sometimes observed to have a high aspect ratio. Use of the dark-field imaging technique [5] enabled an intergranular amorphous phase to be imaged, and showed that the β-Si_3N_4 grains were generally surrounded by a continuous intergranular

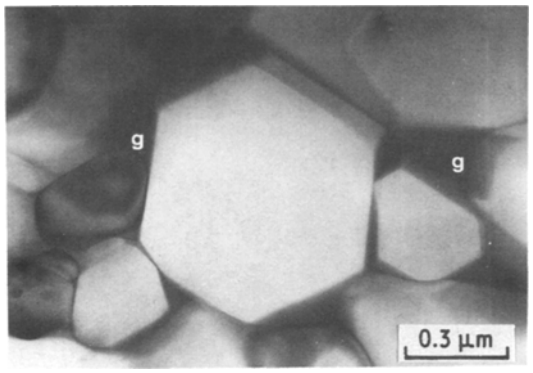

Figure 9 Transmission electron micrograph of partially sintered material showing the strongly varying grain size of the β-Si_3N_4. The dark areas (g) are the glassy phase rich in yttrium, aluminium and silicon.

film which was often as thin as ~ 2 nm along grain boundary facets (Fig. 12). The facet films merged into larger pockets of the same phase at multi-grain junctions. Analyses by STEM/EDX of these glass pockets showed that the amorphous phase in fully sintered material was rich in yttrium, aluminium and silicon.

4. Discussion

4.1. Nitridation

It is evident from the dilatometric and thermogravimetric measurements (Fig. 5) together with X-ray diffractometry (Fig. 6) that the reaction path during nitridation commences with the reaction of sintering aids (primarily Y_2O_3) with the surface silica on the Si_3N_4 and silicon powder particles. This reaction apparently initiates prior to the onset of nitridation of the silicon powder, and promotes nitridation by giving the nitrogen gas access to the silicon. It was found in early investigations that nitridation of powder compacts without additions of sintering aids (Y_2O_3 and Al_2O_3) started at a higher temperature, and required about twice as long at temperature to achieve full conversion of silicon to Si_3N_4 [6]. This provides clear evidence that both initiation and the overall rate of nitridation are enhanced by the presence of sintering aids. Without sintering aids the possible reaction for removal of the silica barrier is $Si + SiO_2 \rightarrow 2SiO(g)$, but in doped powder compacts as used here other reactions are possible within the Y_2O_3–Al_2O_3–SiO_2 system [7, 8]. In the composition studied here the first secondary phase to form during nitridation is Y_2SiO_5 (see Fig. 6).

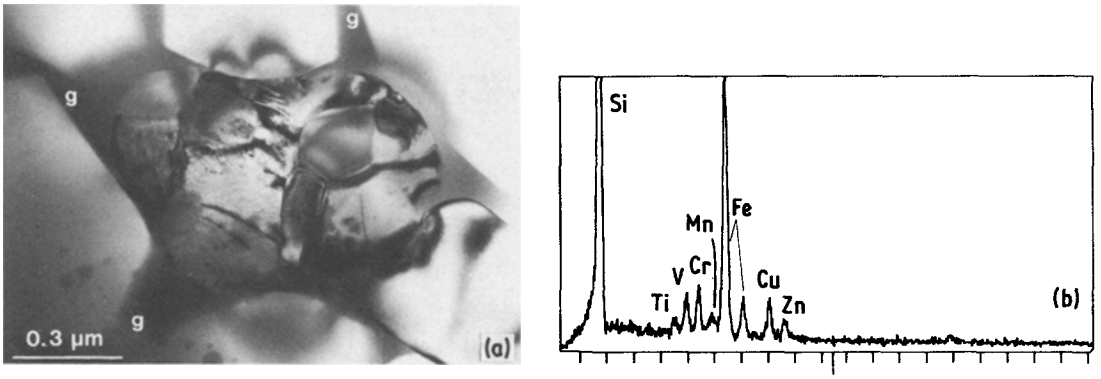

Figure 10 Fine-grained microstructural feature with a high proportion of impurities observed in large glass pockets in partially sintered material. The surrounding glassy phase (g) did not contain any detectable amounts of impurities: (a) transmission electron micrograph; (b) EDX spectrum from the fine-grained feature in (a). Note the high iron content, which originates from the silicon starting powder. The copper and zinc peaks come from the specimen support ring.

After the initial formation of this silicate, Y–N–apatite is rapidly formed, and it could be seen from X-ray diffractograms that Y_2O_3 disappears completely during the first constant-temperature stage (1215° C, see Fig. 5), of the temperature–time schedule. The rapid formation of Y–N–apatite terminates when the added Y_2O_3 is consumed, suggesting that the Y_2O_3 is kinetically involved in this reaction.

In addition to the formation of secondary crystalline phases (i.e. Y_2SiO_5 and Y–N–apatite) there is clear microstructural evidence (Figs. 2, 3, 4 and 7) that amorphous phases are present in nitrided bodies. It was found that the volume fraction of amorphous areas increased during the nitridation sequence and also that the amount of amorphous material in fully nitrided bodies increased with nitridation temperature. Microanalysis by STEM/EDX of thin foils taken from compacts nitrided at different temperatures in the interval 1260 to 1400° C could only detect silicon in the amorphous areas surrounding what was considered to be pores in the microstructure. This indicates that these regions could possibly be formed by, for example, the condensation of SiO(g) to form either asomorphous silica or amorphous Si_2Ni_2O on the pore walls during the nitridation process. The presence of a silicon-rich liquid due to the impurity content of the starting silicon powder [2, 9] could also result in the same microstructural appearance, especially at higher temperatures.

Despite the fact that aluminium was not detected in any of the phases present after nitridation, it seems likely that Al_2O_3 does take part in the early formation of a liquid in the Al_2O_3–SiO_2–Y_2O_3 system where the lowest liquidus temperature is 1345° C [7, 8]. There are indications that the temperature for liquid formation is further lowered to 1300 to 1320° C in the quaternary system which is obtained when Si_3N_4 is included [10]. The observed change

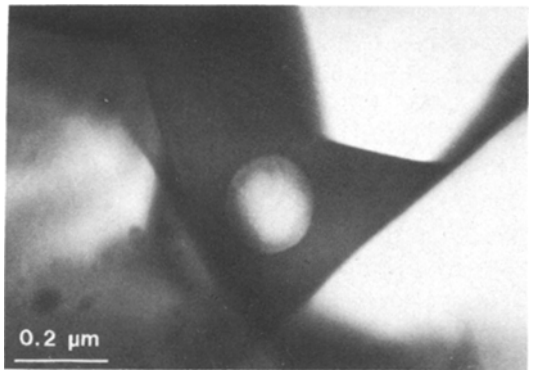

Figure 11 Small β-Si_3N_4 grain with rounded shape in a glass pocket in partially sintered material.

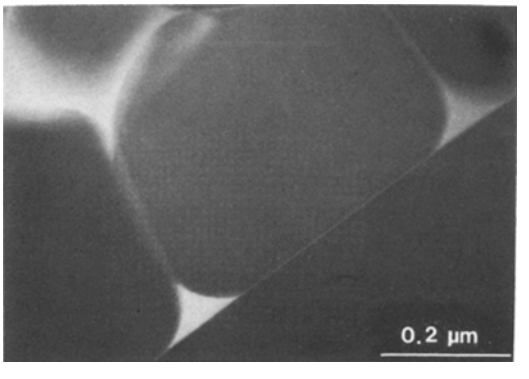

Figure 12 Centred dark-field image of the glassy phase in fully sintered material. The intergranular glass film is in this case approximately 2 nm thick.

in the $Y_2SiO_5/(Y_2SiO_5 + Y$–N–apatite) peak height ratio when the nitridation temperature of 1350° C is reached in the temperature–time programme could be caused by the appearance of such a liquid phase field when the temperature is raised from 1215 to 1350° C. The observed amorphous intergranular films between some of the Si_3N_4 grains (Fig. 4) are probably residues of a liquid which was present at the nitridation temperature.

A plausible explanation for the role of sintering aids during the nitridation process is therefore that Y_2O_3 is mainly active in removing the silica layer from the silicon and Si_3N_4 powder particles to form secondary crystalline phases, while Al_2O_3 probably participates in the early formation of a liquid phase.

During nitridation at 1350° C, the $\alpha/(\alpha + \beta)$ ratio in partially nitrided compacts decreases steadily as the conversion of silicon to Si_3N_4 proceeds. This indicates that β-Si_3N_4 is formed in excess of α-Si_3N_4 during nitridation at this temperature. In early experiments [11] it was found that powder compacts which did not contain additions of sintering aids, and which were nitrided according to a similar time–temperature schedule as that used for nitridation at 1350° C, exhibited a considerably higher $\alpha/(\alpha + \beta)$ peak height ratio than the nitrided compacts in the present investigation. Thus it can be concluded that the formation of β-Si_3N_4 during nitridation at this temperature is strongly affected by additions of sintering aids. It has been found that prolonged holding times beyond that necessary for complete nitridation at temperatures in the range 1260 to 1350° C do not affect the relative proportions of α- and β-Si_3N_4 [6]. Thus is seems that the presence of the previously mentioned Y–Al–Si–O–N liquid does not promote any significant transformation of α to β at temperatures up to 1350° C.

At temperatures higher than 1350° C the relative proportion of α-Si_3N_4 in fully nitrided material drops significantly (see Fig. 1). At these temperatures some melting of silicon occurs, mainly because of iron impurities in the silicon starting powder [2, 9]. The increased relative amount of β-Si_3N_4 can therefore be interpreted either in terms of an increased proportion of the newly formed Si_3N_4 being β-phase, or in terms of transformation of α to β in the presence of this liquid phase [12].

The TEM observations of fine Si_3N_4 grains at the surfaces of partially nitrided silicon powder particles and also at tunnel walls penetrating these grains (Fig. 8) are in agreement with previous work on nitridation of silicon [13, 14]. When the free surface of silicon powder particles is exposed to nitrogen gas at high temperatures, Si_3N_4 nucleates and grows resulting in the formation of a surface layer of Si_3N_4 on the silicon grains. This reaction requires the diffusion of silicon to the growing Si_3N_4 nuclei, and the mass transport of silicon may result in the formation of pores at the surface of the silicon powder particles. Diffusion can then cause a further growth of these pores until they become the "tunnels" shown in Fig. 8. The walls of these tunnels then serve as new nucleation and growth sites for Si_3N_4. As in the case of the previously mentioned silicon-rich amorphous layer on pore walls, the amorphous layer which was observed to be covering the fine-grained structure could be due either to the formation of amorphous silica (by condensation of SiO(g)) or to the formation of amorphous Si_2N_2O during nitridation.

The limited shrinkage of powder compacts which occurs between 1050 and 1215° C during the nitridation programme (see Fig. 5) was also found to occur when heating the powder compacts through the same temperature programme but in an argon atmosphere. Similar dilatometric curves in this temperature range were obtained in the absence of sintering aids and also for semiconductor grade silicon powder [6]. It therefore seems that this shrinkage is due to sintering of the silicon powder particles during the early stages of nitridation.

The reaction sequence during nitridation of Si–Si_3N_4 powder compacts containing additions of Y_2O_3 and Al_2O_3 would thus seem to be the following:

(a) reaction of surface silica with the sintering aids, mainly Y_2O_3, to form secondary phases and thus expose free silicon surfaces;

(b) the silicon particles sinter slightly in the temperature interval 1050 to 1215° C in the early stages of nitridation;

(c) Si_3N_4 forms to a significant extent at the silicon powder surfaces and at tunnel walls extending into the interior of these powder particles;

(d) the early formation of Si_3N_4 decelerates the sintering of silicon; and

(e) slow shrinkage occurs during the main nitridation at 1350° C because of some liquid phase sintering of Si_3N_4.

4.2. Sintering

It was found that α-Si_3N_4 transformed to β-Si_3N_4 during the very early stages of sintering. This rapid transformation of α to β is most probably due to the very fine Si_3N_4 grain size of the material before sintering. In addition to the transformation of α to β, small β-Si_3N_4 grains dissolved in the liquid phase sintering medium in favour of growing columnar β grains which had the characteristic equilibrium hexagonal-shaped cross-section. Despite the non-uniform grain size of the as-nitrided material this process resulted in a uniform final microstructure. The secondary crystalline phases, yttrium silicate and Y–N–apatite which formed during nitridation were found to disappear during sintering.

It is generally thought that a major part of the mass transport required for densification of Si_3N_4 during sintering is associated with the transformation of α-Si_3N_4 to β-Si_3N_4 by solution/reprecipitation in the liquid phase [15, 16]. In the present work this transformation was found to be complete when only $\sim 80\%$ of the theoretical density had been reached. Thus, most of the densification which took place during sintering was not associated with the transformation of α-Si_3N_4 to β-Si_3N_4. It therefore seems likely that the major part of the shrinkage which occurs at the sintering temperature is largely due to a combination of Ostwald ripening and coalescence. Thus the α- to β-Si_3N_4 transformation does not provide the only reaction path for obtaining a uniform fine-grained microstructure. An equally fine and homogeneous microstructure can also be attained by the above mechanisms.

It was noted by STEM/EDX that occasional fine-grained crystalline features (Fig. 10) in the microstructure were rich in impurity elements, especially iron. It can be expected that these features should be eliminated from the microstructure by use of higher-purity silicon starting powders. Some experiments have indeed been carried out where high-purity silicon powder was used in the starting powder mixture [6]. Complete nitridation was obtained and the final sintered product had the same high density as that in the present work.

4.3. The final sintered product

The microstructure of the fully sintered product (Fig. 12) which results from this method of fabrication is very similar to that of Si_3N_4 materials produced by conventional pressureless sintering of fine Si_3N_4 powders with additions of Y_2O_3 and Al_2O_3 as sintering aids [11]. The β-Si_3N_4 grains in the final product had a relatively uniform grain size, with the diameters of their characteristic hexagonal-shaped cross-sections being in the range 0.3 to 0.5 μm. Many grains had a high aspect ratio. As in conventional polyphase Si_3N_4 materials, the β-Si_3N_4 grains were surrounded by a thin intergranular amorphous phase.

As of yet no attempts have been made to optimize the amount or composition of the amorphous phase present in the final microstructure of materials fabricated by this technique. Clearly there is ample scope for doing this and also for making use of other principles of "ceramic alloying" such as, for example, those used in the production of β'SiAlON materials [17].

5. Conclusions

(a) Fully dense fine grained β-Si_3N_4 material with a microstructure similar to that of conventional pressureless sintered Si_3N_4 can be fabricated by the nitridation and subsequent pressureless sintering of Si : Si_3N_4 powder compacts containing additions of Y_2O_3 and Al_2O_3.

(b) Nitridation of the silicon in the powder compacts to Si_3N_4 is promoted by sintering aids (Y_2O_3 and Al_2O_3) which react with surface silica on the powder particles to form secondary phases.

(c) Both α- and β-Si_3N_4 are formed during the nitridation of silicon to Si_3N_4. The proportion of β phase formed increases during the nitriding process, and the β content in fully nitrided compacts increases at higher nitridation temperatures.

(d) During nitridation extremely fine-grained Si_3N_4 forms at silicon powder particle surfaces, and at tunnel walls extending into the interior of these powder particles.

(e) Some densification occurs during nitridation.

(f) Complete transformation of α-Si_3N_4 to β-Si_3N_4 takes place at the onset of pressureless sintering of the nitrided compacts.

(g) The crystalline secondary phases (yttrium silicate and Y–N–apatite) which form during nitridation are eliminated from the microstructure during the pressureless sintering of nitrided powder compacts.

(h) The fine-grained fully sintered microstructure is mainly achieved during sintering by a combination of Ostwald ripening and coalescence.

Acknowledgements

This work was supported by the Swedish Board for Technical Development and the Swedish Natural Science Research Council. Discussions with Dr F. F. Lange are gratefully acknowledged.

References

1. R. POMPE, L. HERMANSSON and R. CARLSSON, *Sprechsaal* **115** (1982) 1098.
2. *Idem,* "Engineering with Ceramics", edited by R. W. Davidge (British Ceramic Society, Stoke-on-Trent, 1982) p. 65.
3. A. ATKINSON, P. J. LEATT and A. J. MOULSON, *J. Mater. Sci.* **7** (1972) 482.
4. C. P. GAZZARA and D. R. MESSIER, *Ceram. Bull.* **59** (1977) 777.
5. D. R. CLARKE, *Ultramicros.* **4** (1979) 33.
6. R. POMPE, manuscript in preparation.
7. G. WÖTTING and G. ZIEGLER, Proceedings of the 5th CIMTEC Conference, Lignano Sabbiadoro, Italy, June, 1982, edited by P. Vincenzini (Elsevier, Amsterdam, 1983) p. 951.
8. I. A. BONDER and F. J. GALAKOV, *Izv. Akad. Nauk SSR, Ser. Khim.* **7** (1964) 1325.
9. S. M. BOYER and A. J. MOULSON, *J. Mater. Sci.* **13** (1978) 1637.
10. R. POMPE, L. EKLUND and L. HERMANSSON, "Special Ceramics", Vol. 7, edited by D. Taylor and P. Popper (British Ceramic Society, Stoke-on-Trent, 1981) p. 97.
11. R. POMPE, L. K. L. FALK and G. L. DUNLOP, manuscript in preparation.
12. P. E. D. MORGAN, *J. Mater. Sci.* **15** (1980) 791.
13. A. ATKINSON, A. J. MOULSON and E. W. ROBERTS, *J. Amer. Ceram. Soc.* **59** (1976) 285.
14. A. ATKINSON, P. J. LEATT, A. J. MOULSON and E. W. ROBERTS, *J. Mater. Sci.* **9** (1974) 981.
15. S. HAMPSHIRE and K. H. JACK, "Special Ceramics", Vol. 7, edited by D. Taylor and P. Popper (British Ceramic Society, Stoke-on-Trent, 1981) p. 37.
16. M. H. LEWIS and R. J. LUMBY, *Powd. Metall.* **26** (1983) 73.
17. M. H. LEWIS, A. R. BHATTI, R. J. LUMBY and B. NORTH, *J. Mater. Sci.* **15** (1980) 103.

Received 3 September
and accepted 2 November 1984